



1 A Global Ozone Profile Climatology for Satellite Retrieval
2 Algorithms Based on Aura MLS Measurements and the
3 MERRA-2 GMI Simulation

4
5
6 Jerald R. Ziemke^{1,2}, Gordon J. Labow³, Natalya A. Kramarova¹, Richard D. McPeters¹, Pawan
7 K. Bhartia¹, Luke D. Oman¹, Stacey M. Frith³, David P. Haffner³

8
9 ¹ NASA Goddard Space Flight Center, Greenbelt, Maryland, USA

10 ² Morgan State University, Baltimore, Maryland, USA

11 ³ SSAI, Lanham, Maryland, USA

12
13 **Abstract.** A new atmospheric ozone profile climatology has been constructed by combining
14 ozone profiles from the Aura Microwave Limb Sounder (MLS) and Modern-Era Retrospective
15 Analysis for Research Applications version 2 (MERRA2) Global Modeling Initiative (GMI)
16 model simulation (M2GMI). The MLS and M2GMI ozone profiles are merged between 13 and
17 17 km (~159 and 88 hPa) with MLS used for stratospheric and GMI for primarily tropospheric
18 levels. The time record for profiles from MLS and GMI is August 2004-December 2016. The
19 derived seasonal climatology consists of monthly zonal-mean ozone profiles in 5-degree latitude
20 bands from 90°S-90°N covering altitudes (in Z* log-pressure altitude) from zero to 80 km in 1
21 km increments. This climatology can be used as a priori information in satellite ozone retrievals,
22 in atmospheric radiative transfer studies, and as a baseline to compare with other measured or
23 model-simulated ozone. The MLS/GMI seasonal climatology shows a number of improvements
24 compared to previous ozone profile climatologies based on MLS and ozonesonde measurements.
25 These improvements are attributed mostly to continuous daily global coverage of GMI
26 tropospheric ozone compared to sparse regional measurements from sondes. Only daytime
27 measurements for MLS are used in the MLS/GMI climatology compared to the previous
28 MLS/sonde climatology that averaged MLS day and night measurements together; the daytime-
29 only measurements are important for applications involving the upper stratosphere and lower



30 mesosphere where the ozone diurnal cycle is large. In addition to the seasonal climatology, we
31 also derive an additive climatology to account for inter-annual variability in stratospheric zonal-
32 mean ozone profiles which is based on a rotated empirical orthogonal function (REOF) analysis
33 of Aura MLS ozone profiles. This REOF climatology starts in 1970 and captures most of the
34 inter-annual variability in global stratospheric ozone including Quasi-Biennial Oscillation (QBO)
35 signatures.

36

37 **1. Introduction.**

38

39 McPeters and Labow (2012) (hereafter, ML) and Labow et al. (2015) combined ozone profile
40 data from ozonesondes and the Aura Microwave Limb Sounder (MLS) (Livesey et al., 2011) to
41 use as climatological a priori information for satellite retrievals of ozone. These ozone profile
42 climatologies were constructed by merging ozonesondes in the troposphere with satellite ozone
43 in the stratosphere/mesosphere. For the ML climatology the stratosphere/mesosphere portion of
44 the climatological ozone profiles was based on MLS daytime limb measurements.

45

46 The limited amount and sparse spatial coverage of ozonesonde data has led us to now use the
47 NASA Goddard Earth Observing System (GEOS) Global Modeling Initiative (GMI) model as a
48 substitute for the ozonesonde data in the lower atmosphere. The GMI model uses Modern-Era
49 Retrospective Analysis for Research Applications version 2 (MERRA2) meteorology. We refer
50 to this as the MERRA2 GMI (hereafter M2GMI) model.

51

52 We have generated a new ozone profile seasonal climatology based on combining MLS v4.2 and
53 M2GMI ozone profiles which represents an improvement from our previous sonde-satellite
54 ozone climatologies including ML. The earlier climatologies were binned in 10-degree latitude
55 bands due mostly to the limited coverage of sondes. In contrast, the new MLS/GMI ozone
56 profile climatology has been binned to 5° latitude bands by taking advantage of better spatial and
57 temporal coverage of the model output. This new climatology also extends to 80 km in altitude
58 compared to 65 km in the previous climatologies.

59



60 We also generated a new inter-annual ozone profile climatology that is based on MLS ozone,
61 SBUV total ozone, and rawinsonde wind data using a rotated empirical orthogonal function
62 (REOF) method. The application of the MLS/GMI seasonal climatology by itself or together
63 with this REOF inter-annual climatology as a priori enables more accurate profile and column
64 ozone retrievals, including improvements for inter-calibrating and merging independent satellite
65 ozone measurements such as for the SBUV Merged Ozone Dataset (MOD) (Frith et al., 2014).

66

67 In the following sections we describe the data and GMI model output used in our analysis,
68 outline the methods used to construct the MLS/GMI seasonal climatology and REOF
69 climatology, and discuss the properties of the climatologies. We conclude with a summary of
70 our results. Additional details and figures not covered in the main text are included in a
71 Supplementary Material section.

72

73 **2. Ozone data and M2GMI model simulated ozone.**

74

75 **2.1. Aura MLS Ozone.**

76

77 The Microwave Limb Sounder (MLS) instrument onboard the Aura spacecraft makes ozone
78 profile measurements along the orbital track in both daytime and nighttime. Aura is in a sun
79 synchronous orbit, and therefore MLS has nearly complete latitude coverage each day between
80 82°S and 82°N, with local equatorial crossing times of approximately 1:45 pm for the ascending
81 sunlit portion of the orbit and 1:45 am for the nighttime descending node.

82

83 The MLS instrument is a thermal-emission microwave limb sounder that measures vertical
84 profiles of mesospheric, stratospheric, and upper tropospheric temperature, ozone, and several
85 other trace gases from limb scans made ahead of Aura about 7 minutes before the satellite
86 reaches the same point directly below. The MLS instrument primarily uses the 240 GHz
87 microwave band for v4.2 ozone retrievals which for recommended scientific applications extend
88 from 0.0215 hPa to 261 hPa on 38 pressure layers. Vertical spacing for these layers is about 1.3
89 km everywhere below 1 hPa and about 2.7 km at most altitudes above 1 hPa. By comparison,
90 the vertical resolution for the ozone retrievals is reported to be ~3 km extending from 261 hPa up



91 into the mesosphere. Further details regarding the MLS measurements are described by Livesey
92 et al. (2011). The time record for the MLS ozone used in our study was August 2004 –
93 December 2016. Given the high quality of MLS ozone in the low mesosphere we extend the
94 climatology to 80 km from 65 km where the ML climatology ended. We use only the daytime
95 measurements ($SZA < 90^\circ$) from MLS in ozone profile climatology since the daytime data is most
96 appropriate for many passive UV/Vis ozone remote sensing techniques that require daytime
97 measurements. A number of studies of the diurnal ozone variations in stratospheric and
98 mesospheric ozone [Parrish et al., 2014; Frith et al., 2020, and references therein] demonstrated
99 sizeable diurnal ozone variations around 5-10 hPa.

100

101 **2.2. SBUV MOD total ozone record.**

102

103 We use total column ozone measurements from the Solar Backscatter UltraViolet (SBUV) v8.6
104 merged ozone dataset (MOD) as a proxy to reproduce time-dependent inter-annual variability for
105 the REOF climatology described in section 4. The MOD total ozone dataset (Frith et al., 2014)
106 is comprised of a composite set of measurements from several SBUV instruments. The first
107 instrument was Nimbus-4 BUV launched in 1970, followed by the second and improved version
108 SBUV on Nimbus-7 launched in October 1978. Starting in 1989, seven SBUV/2 instruments
109 were launched beginning with NOAA-9, followed by NOAA 11, 14, 16, 17, 18, and 19. Now
110 this record is extended with the Ozone Mapping and Profiler Suite (OMPS) nadir-profiler (NP)
111 on board the Suomi National Polar-orbiting Partnership (SNPP) satellite. There are four follow-
112 up OMPS instrumental suites as a part of JPSS program (with JPSS-1/NOAA-20 already in
113 operation) that will extend the SBUV-type ozone observations in the next two decades. The
114 SBUV instruments retrieve broad ozone profiles from measurements of backscattered solar UV
115 radiation which can be integrated to give total column ozone. All MOD instrument
116 measurements have been processed using the v8.6 retrieval algorithm as described by McPeters
117 et al. (2013) and Bhartia et al. (2013). In this study we use monthly zonal-mean gridded total
118 ozone extending from 90°S to 90°N at 5° latitudinal binning (Frith, 2021, personal
119 communication). The MOD ozone record spans from January 1970 to December 2020 with
120 some temporal gaps, including May 1976-October 1978 due to missing Nimbus-4 BUV
121 measurements.



122

123 **2.3. Ozonesonde measurements.**

124

125 We include balloon-launched ozonesonde measurements for comparison and validation of the
126 M2GMI simulated tropospheric ozone. The ozonesonde database extends from 2004-2019 and
127 includes measurements from the Southern Hemisphere Additional OZonesondes (SHADOZ)
128 program (Thompson et al., 2017; Witte et al., 2017), the World Ozone and Ultraviolet Data
129 Center (WOUDC) (<https://woudc.org/>), and the Network for the Detection of Atmospheric
130 Composition Change (NDACC). (<http://www.ndsc.ncep.noaa.gov/>). The ozonesondes provide
131 daily ozone profile concentrations as a function of altitude from several dozen global sites. The
132 ozone profiles are integrated vertically each day from surface to tropopause to derive
133 tropospheric column ozone (TCO) measurements using the same tropopause pressures as used
134 for M2GMI TCO. Tropopause pressure for both sonde and GMI TCO measurements was
135 derived from National Centers for Environmental Prediction (NCEP) re-analyses based on the
136 World Meteorological Organization (WMO) 2K km⁻¹ temperature lapse-rate definition. Most all
137 of the sonde ozone profile measurements that we use are from Electrochemical Concentration
138 Cell (ECC) instruments.

139

140 In section 4 we describe construction of the REOF inter-annual ozone profile climatology that
141 includes monthly tropical Quasi-Biennial Oscillation (QBO) zonal winds in its construction. The
142 tropical QBO zonal winds come from the Maldives (January 1970 - December 1975) and
143 Singapore (January 1976 - present) rawinsonde record (Univ. Berlin, <https://www.geo.fu-berlin.de/met/>).

144

146 **2.4. MERRA-2 GMI simulated ozone.**

147

148 The M2GMI simulation is produced with the Goddard Earth Observing System (GEOS)
149 modeling framework (*Molod et al.*, 2015), using winds, temperature, and pressure from the
150 MERRA-2 reanalysis (*Gelaro et al.*, 2017). The configuration for this study is a dynamically
151 constrained replay (*Orbe et al.*, 2017) coupled to the Global Modeling Initiative's (GMI)
152 stratospheric and tropospheric chemical mechanism (*Duncan et al.*, 2007; *Oman et al.*, 2013;



153 *Nielsen et al.*, 2017). The simulation was run at $\sim 0.5^\circ$ horizontal resolution, on the cubed sphere,
154 and output on the same 0.625° longitude x 0.5° latitude grid as MERRA-2 from 1980-2016. We
155 refer to Strode et al. (2015, 2020) for details of the M2GMI model simulation. The daily
156 M2GMI ozone profiles were averaged monthly and re-gridded from the original resolution to
157 zonal means in 5° latitude bands; the original 72 layers of the simulated profile ozone were also
158 re-mapped to Z^* altitudes with 1 km vertical spacing (section 3.2).

159

160 **2.4.1. Evaluation of M2GMI simulated tropospheric ozone.**

161

162 Ozone profiles generated by the M2GMI simulation have been extensively evaluated in a
163 number of studies. Stauffer et al. (2019) provides a detailed global analysis of M2GMI ozone
164 profiles using comparisons with ozonesondes. On average they found differences of about $\pm 5\%$
165 between M2GMI and sondes in the troposphere from 38 sonde stations from 69°S - 79°N (their
166 Fig. 1). The largest differences were in the tropics where M2GMI was lower than sonde by up to
167 10-20% in low-mid troposphere, but in the tropical tropopause region M2GMI was higher than
168 sonde by 40-50%; the large percentage differences however can be due to relatively low mean
169 background ozone concentrations of only ~ 1 - 2 DU km^{-1} . Wargan et al. (2018) compared the
170 annual mean ozone mixing ratio anomalies for 1998-2016 between sondes and M2GMI at
171 several stations for 70 hPa, 100 hPa, and 200 hPa. Their comparisons show squared correlations
172 varying from 0.62 to 0.93 and they concluded that the M2GMI simulation well captures the
173 variability of tropospheric ozone including the UTLS region. Ziemke et al. (2014) provide
174 additional evaluation of M2GMI tropospheric ozone by comparing with ozonesondes, satellite,
175 and Global Modeling and Assimilation Office (GMAO) data assimilation; the M2GMI and sonde
176 daily comparisons from tropics to high latitudes in both hemispheres (their Figs. 2-7) showed
177 offsets and difference standard deviations varying ~ 0 - 2 DU (~ 0 - 7%) and 4 - 7 DU (~ 15 - 23%),
178 respectively. The M2GMI simulated ozone profiles have also been extensively compared with
179 Atmospheric Tomography Mission (ATom) aircraft flight measurements (Bourgeois et al., 2020)
180 for years 2015 and 2016 (Junhua Liu, personal communication, 2020). The ATom in-flight
181 measurements of ozone volume mixing ratio are found to compare closely with M2GMI
182 simulated ozone, generally within about $\pm 20\%$ along each of the mission flight paths that
183 included meandering ascent and descent between near surface and tropopause each day.



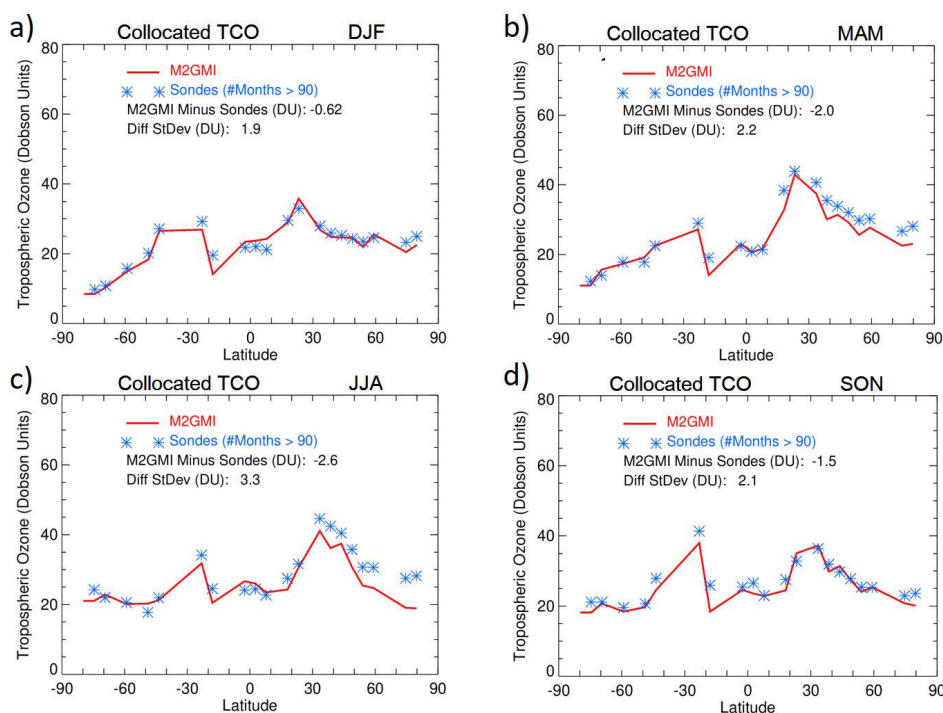
184

185 Our study also includes evaluation of M2GMI simulated tropospheric ozone. Figure 1 compares
186 sonde and M2GMI Tropospheric Column Ozone (TCO) where the sonde and M2GMI
187 measurements have been space-time co-located at the sonde station sites and seasonally averaged
188 for 2004-2016. As noted in section 2.3, both sonde and M2GMI TCO are derived using the same
189 NCEP WMO tropopause pressures.

190

191 The M2GMI modelled ozone in Fig. 1 closely simulates the sonde measured ozone year-round
192 with an exception in the NH mid-high latitudes in MAM and JJA where the simulation tends to
193 underestimate sonde TCO by ~5 DU or more. Section S1 of the Supplementary Material
194 includes additional discussion and figures regarding evaluation of M2GMI tropospheric ozone
195 profiles using ozonesondes and surface lidar measurements.

196



197

198 **Figure 1.** Comparisons between M2GMI simulated (red curves) and ozonesonde TCO (blue
199 asterisks) averaged over three-month seasons (indicated) for 2004-2016. The M2GMI TCO field



200 is sampled daily at the sonde station locations. All TCO is in Dobson Units. The same daily
201 tropopause is used for both M2GMI and sonde to derive TCO, and is defined as according to the
202 WMO 2 K km⁻¹ lapse-rate tropopause definition using NCEP temperatures. Included in each
203 panel are mean offsets and standard deviations of TCO seasonal differences.

204

205 **3. The MLS/GMI seasonal climatology.**

206

207 The MLS/GMI seasonal climatology product is derived for both volume mixing ratio (units
208 ppmv) and vertical column concentration (DU km⁻¹); the latter has vertical and latitudinal
209 structure that is closely similar to that of ozone number density and ozone partial pressure.
210 Standard deviations are reported for both mixing ratios and column concentrations based upon
211 all available daily ozone profiles over a given month and within every 5° latitude band. The
212 standard deviations provide a measure of climatological ozone variability and are important for
213 error covariance matrices included as a priori information in retrieval algorithms such as the
214 optimal estimation method of Rodgers (2000). We refer the reader to the Supplementary
215 Materials for further discussion and figures involving calculated standard deviations.

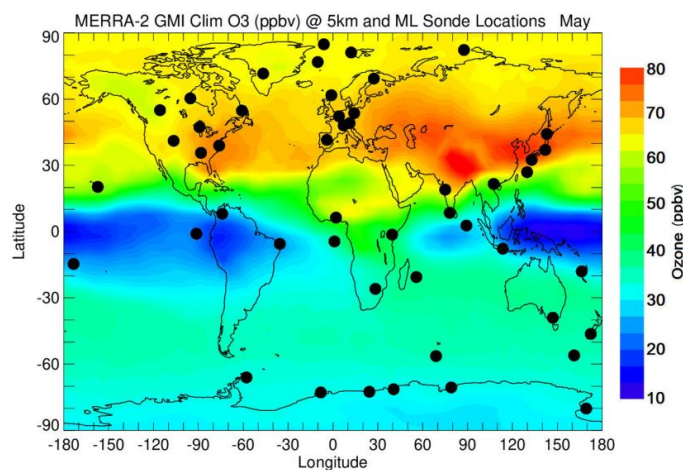
216

217 **3.1. Global coverage of M2GMI tropospheric ozone compared to sondes.**

218

219 Our motivation for using M2GMI simulation is that they provide better spatial and temporal
220 representation of tropospheric ozone profiles than ozonesondes. The sondes are sparsely
221 distributed over the Earth with generally only a few measured profiles per month for a given
222 station. The limited spatial coverage of sondes is demonstrated in Fig. 2 with M2GMI mid-
223 tropospheric ozone concentration (ppbv) at height $Z^*=5$ km for climatological May (Z^* is
224 approximately equal to actual altitude and is defined in section 3.2.)

225



226

227 **Figure 2.** Map of climatological ozone volume mixing ratio (in ppbv) from the M2GMI
228 simulation at $Z^* = 5$ km altitude (see section 3.2) for the month of May. Blue color indicates areas
229 with ozone concentration of about 10 ppbv and red color corresponds to regions with > 75 ppbv.
230 Black circles show locations of the sonde stations with a long observational record. Data from
231 these stations were used to constrain tropospheric ozone profiles in the ML climatology.

232

233 Tropospheric ozone exhibits planetary-scale variability that includes a year-round zonal wave-1
234 pattern in the tropics (greatest amplitude in September-October) and large-scale patterns outside
235 the tropics that vary greatly with season and region (Fishman et al., 1990). The tropical wave-1
236 in tropospheric ozone originates from regional sources of ozone: lightning, biofuel & biomass
237 burning, stratosphere-troposphere exchange (STE), and transport associated with the tropical
238 east-west Walker circulation. In the extra-tropics, the large planetary scale features in
239 tropospheric ozone have strong seasonal dependence with the seasonal maximum in JJA in the
240 NH and SON in the SH. These seasonal patterns in tropospheric ozone outside the tropics are
241 also due to combined effects from STE, biofuel, lightning, biomass burning, and long-range
242 transport. The global planetary-scale patterns in tropospheric ozone columns were first shown
243 from TOMS/SAGE (Fishman et al., 1990) and TOMS/MLS (Ziemke et al., 1996) satellite
244 measurements. The patterns in the M2GMI tropospheric ozone mixing ratio for $Z^* = 5$ km in
245 Fig. 2 in the tropics and in the NH are similar to the satellite TCO patterns during May.

246



247 It is apparent from Fig. 2 that the ensemble of ozonesondes is unlikely to effectively represent
248 the zonal mean tropospheric ozone values due to their limited sampling. For example, in the
249 tropics the sonde measurements under-sample the tropical wave-1 structure in tropospheric
250 ozone. Due to the under-sampling in the tropical Pacific area, sondes do not capture the very
251 low ozone concentrations of ~10 ppbv. This leads to the over-estimation of zonal-mean
252 tropospheric ozone in the tropics from the sondes. We will show later that this over-
253 determination of ML tropospheric ozone in the tropics averages to about 5-10 DU in TCO year-
254 round between 20°S-20°N. The sondes also tend to miss the high values of ozone in the NH
255 mid-latitudes over the Asian continent (see Fig. 2), thus introducing a low bias in zonal-mean
256 tropospheric ozone in NH mid-latitudes.

257

258 **3.2. Merging MLS and M2GMI ozone profiles.**

259

260 Simulated ozone values from the M2GMI model were merged with ozone measurements from
261 MLS to construct an ozone profile seasonal climatology in the format of monthly zonal means.
262 For low and mid-latitudes between 40°N and 40°S the M2GMI and MLS profiles were merged
263 for Z^* levels between 13 km and 21 km (156 hPa to 49 hPa). For latitudes poleward of 40° in
264 each hemisphere the profiles were merged slightly lower in the atmosphere, for Z^* levels
265 between 8 km and 16 km (320 hPa to 101 hPa). Within the merged altitude ranges the
266 climatology is weighted linearly, from 100% M2GMI at the lowest altitude to 100% MLS at the
267 highest altitude. Standard deviations were calculated for each climatological ozone value.

268

269 As in previous climatologies, the altitude variable used for our climatology is Z^* , a parameter
270 frequently used in comparisons of atmospheric chemistry models (Park et al., 1999). Z^* is in
271 units of kilometers but can be considered a pressure variable. Z^* (km) is defined by
272 $Z^* = 16 \cdot \log(1013/P)$ where P is atmospheric pressure in units hPa. The altitude spacing for our
273 climatology is 1 km in Z^* units. In an isothermal terrestrial atmosphere Z^* would correspond
274 closely to altitude.

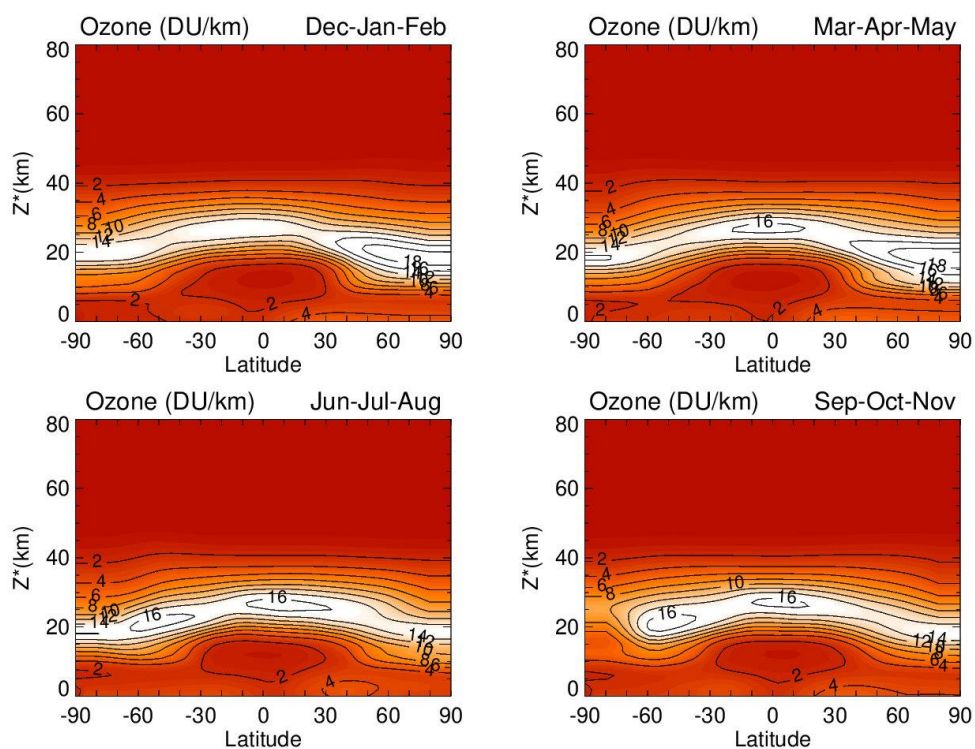
275

276 **3.3. Comparisons with the ML Climatology.**

277



278 We first examine basic global patterns of the MLS/GMI seasonal climatology. Figure 3 shows
279 vertical column concentrations (DU km^{-1}) for the climatology by 3-month season (indicated) for
280 $Z^* = 0\text{--}80$ km. Column concentrations in the low stratosphere in both hemispheres are largest
281 during winter-spring and smallest in summer. In both hemispheres, ozone is largest in the
282 winter-spring months due to seasonal transport from the tropics to the extra-tropics in winter-
283 spring months (i.e., the Brewer Dobson Circulation) and longer lifetimes for ozone in the low
284 stratosphere. The highest ozone amounts in Fig. 3 are $\sim 18\text{--}20 \text{ DU km}^{-1}$ in the NH around 20 km
285 during winter and spring. In the troposphere, very low ozone density of less than 2 DU km^{-1}
286 occurs in the tropics year-round.
287



288
289 **Figure 3.** Meridional cross-sections of derived zonal-mean vertical ozone concentration (units
290 DU km^{-1}) for the MLS/GMI seasonal climatology. This 12-month climatology is averaged over
291 three-month seasons (indicated) for 2004-2016 and is binned for 5° latitude bands and Z^* levels
292 from 0-80 km at 1 km spacing (see text).



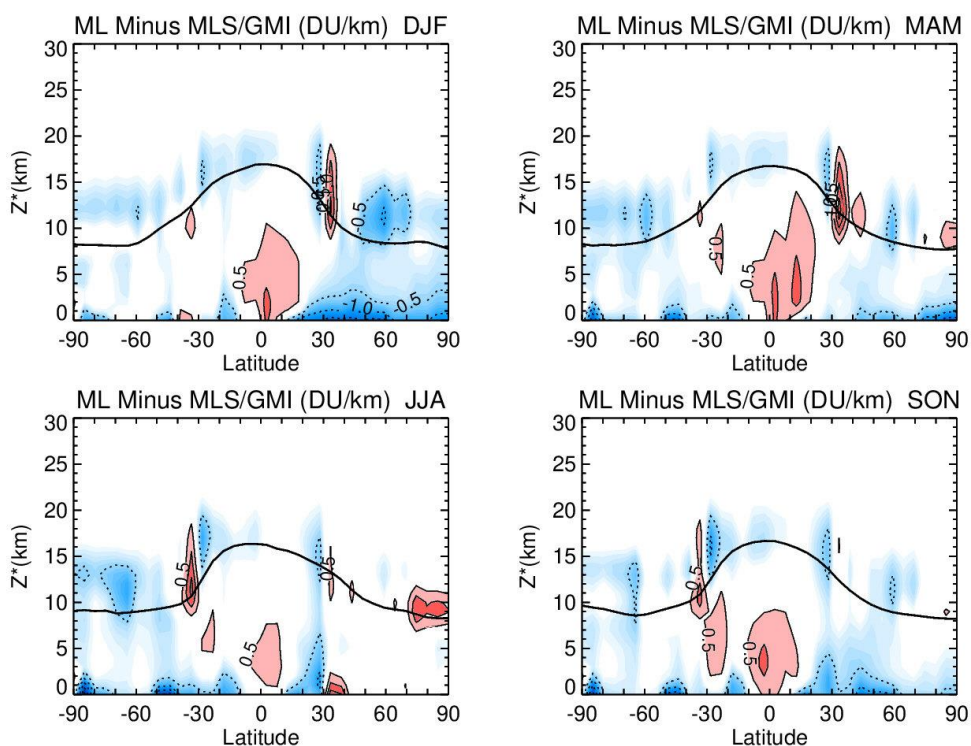
293

294 While the basic characteristics of stratospheric ozone in Fig. 3 are important to note, our main
295 focus is to compare tropospheric ozone in Fig. 3 with the ML sonde ozone climatology. Because
296 the ML climatology uses sparsely sampled sonde measurements to estimate zonal-means in the
297 troposphere, it is possible that there may be substantial differences.

298

299 Figure 4 compares MLS/GMI minus ML zonal-mean column ozone by season, plotted as Z^*
300 altitude versus latitude. Only Z^* levels 0-30 km are included in Fig. 4 to highlight differences in
301 ozone profiles used for the troposphere and the low stratosphere merging region. Year-round
302 positive differences in the tropics in Fig. 4 suggest that ML is always too large in the low-mid
303 troposphere compared to M2GMI due to absence of ML sonde measurements in the Pacific
304 region where tropospheric ozone is low (e.g., Fig. 2). At latitudes around $\pm 35^\circ$ and elsewhere in
305 the low stratosphere merging region in Fig. 4 there are anomalous differences from -0.5 up to
306 $+1.5 \text{ DU km}^{-1}$; these sharp patterns are ascribed to sonde sampling issues for the ML
307 climatology. In the boundary layer throughout the NH extra-tropics during winter (i.e., upper
308 left panel in Fig. 4) the M2GMI ozone is higher than sondes by ~ 0.5 to 1 DU km^{-1} . These latter
309 differences are attributed to a known model issue related to underestimating surface deposition
310 over cold surfaces (Jaegle et al. 2018), most prominent in the NH boundary layer during winter.
311 When compared with ML in Fig. 4, the model over-determines ozone by about 2 DU in DJF.

312



313

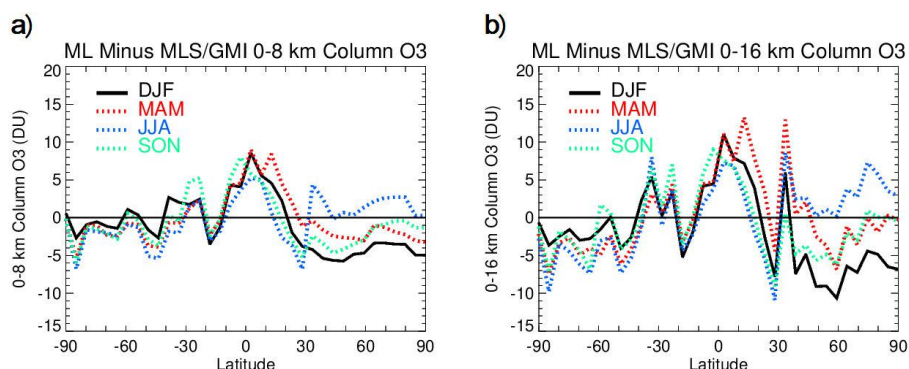
314 **Figure 4.** Meridional cross-sections of ML minus MLS/GMI climatologies of ozone column
315 concentration (DU km^{-1}). These differences are averaged over three-month seasons (indicated)
316 for 2004-2016 and are binned for 10° latitude bands and Z^* levels from 0-30 km at 1 km spacing.
317 Contour levels (indicated) increment by 0.5 DU km^{-1} with blue/dashed contours meaning
318 negative, and pink to red solid contours meaning 0.5 to 1.0 DU km^{-1} or greater. The black line
319 indicates tropopause height according to the WMO 2 K km^{-1} lapse-rate tropopause definition
320 using NCEP temperatures. White color denotes zero differences.

321

322 Line plots of seasonal differences (ML minus MLS/GMI) of integrated ozone columns are
323 shown in Fig. 5 for 0-8 km (Fig. 5a) and 0-16 km (Fig. 5b). These line plots are determined from
324 Fig. 4 by summing the 1 km layers of ML minus MLS/GMI differences. In the tropics 0-16 km
325 integrated column in Fig. 5b represents the total troposphere (i.e., TCO) with ML larger than
326 MLS/GMI by about 10 DU year-round. Comparison with the 0-8 km columns in the left panel
327 show that these differences in the tropics originate mostly from the lower troposphere which is



328 consistent with all four panels in Fig. 4. Outside the tropics in Fig. 5 there are seasonal offset
329 differences in the NH up to -5 to -10 DU during DJF. Part of the reason for the ML minus
330 MLS/GMI seasonal biases in Fig. 5 is due to sonde under-sampling for the ML climatology. The
331 sonde under-sampling also creates the sharp (non-physical) variability seen between adjacent
332 latitude bins in Fig. 5.
333



334
335 **Figure 5.** (a) Line plots of seasonal differences of ML minus MLS/GMI integrated ozone
336 columns for 0-8 km. The differences are averaged over three-month seasons (indicated by DJF,
337 MAM, JJA, and SON). (b) Same as (a), but for 0-16 km ozone columns.

338

339 **4. An inter-annual ozone profile climatology.**

340

341 The MLS/GMI seasonal climatology captures the mean vertical shape of ozone profiles by
342 season and latitude in both troposphere and stratosphere. However, inter-annual processes such
343 as the QBO produce sizeable changes in the vertical ozone distribution in stratospheric ozone
344 from year to year. To capture these variations, we have constructed a global time-dependent
345 climatology of stratospheric ozone that represents ozone inter-annual variability. This
346 climatology can be used either independently or added to the MLS/GMI seasonal climatology,
347 depending on the particular application.

348

349 The inter-annual ozone climatology is constructed using a method that includes an REOF
350 analysis as described by Richman (1986, and references therein). With our approach, vertical
351 information is derived from an REOF analysis of MLS ozone profiles, while time dependence is



352 provided by coupling the ROEF analysis time coefficients with SBUV MOD total ozone and
353 tropical QBO zonal winds. The time period for the ROEF climatology depends on the
354 availability of total ozone and tropical QBO winds. The time period for this climatology is
355 1970-2018 with gaps present due to some missing MOD total ozone including Nimbus 4
356 measurements in the 1970s.

357

358 We demonstrate that the ROEF climatology does very well in capturing inter-annual variability
359 of stratospheric ozone. The excellent vertical resolution of MLS ozone limb measurements of ~3
360 km resolves much of the vertical variability of ozone caused by low-frequency and episodic
361 processes such as the QBO, extra-tropical stratospheric warmings, and year-round planetary-
362 scale wave events (e.g., Ziemke et al., 2014, and references therein). Many nadir instrument
363 ozone profile retrievals have coarse vertical resolution of ~10 km or greater (such as from SBUV
364 or OMI) and cannot do nearly as well at resolving vertical changes in stratospheric ozone.

365

366 We provide a short description of the ROEF method and refer to the Supplementary Materials
367 for details regarding the calculations. The Empirical Orthogonal Function (EOF) method
368 (Kutzbach 1967, and references therein) was applied to MLS ozone anomaly profiles to derive
369 repeatable inter-annual patterns in the ozone vertical distribution. The EOF analysis was applied
370 to monthly zonal mean anomalies derived by removing seasonal cycles in MLS monthly zonal
371 mean profiles between January 2005 and December 2016. Profiles were binned into 5° latitude
372 bands (36 bands for 90°S-90°N) between 1 and 261 hPa (30 pressure levels).

373

374 The main challenge of EOF analysis is interpretation of derived EOFs and their attribution to
375 specific geophysical processes. In this study we applied rotated EOFs which helped us to
376 attribute our EOF results to specific geophysical quantities, that is, total column ozone and
377 equatorial zonal wind. The step-by-step methodology for developing the ROEF-based inter-
378 annual ozone profile anomaly climatology is described in the Supplementary Materials. We used
379 MLS ozone anomalies expressed as ozone partial pressure for the ROEF analysis rather than
380 ozone mixing ratio because it helped to attribute the EOF1 time coefficient directly to total ozone
381 column measurements at all latitudes. The first ROEF vector with the MOD SBUV total ozone
382 time series as a proxy explains about 50-70% of the inter-annual ozone variability. -Next, we



383 derived a second REOF (REOF-2) that we attributed to the QBO and used the equatorial zonal
384 wind time series as a proxy for REOF-2. The sum of these two REOFs explains about 70-80% of
385 the inter-annual variability in de-seasonalized MLS zonal mean ozone profiles. Since only MLS
386 profiles are used to constrain the vertical shapes of the REOFs and time coefficients are
387 described by total ozone and zonal winds, this REOF climatology can be used in the future (even
388 after MLS stops operating) or can be extended into the past to the pre-Aura time period
389 whenever total column ozone and wind data are available.

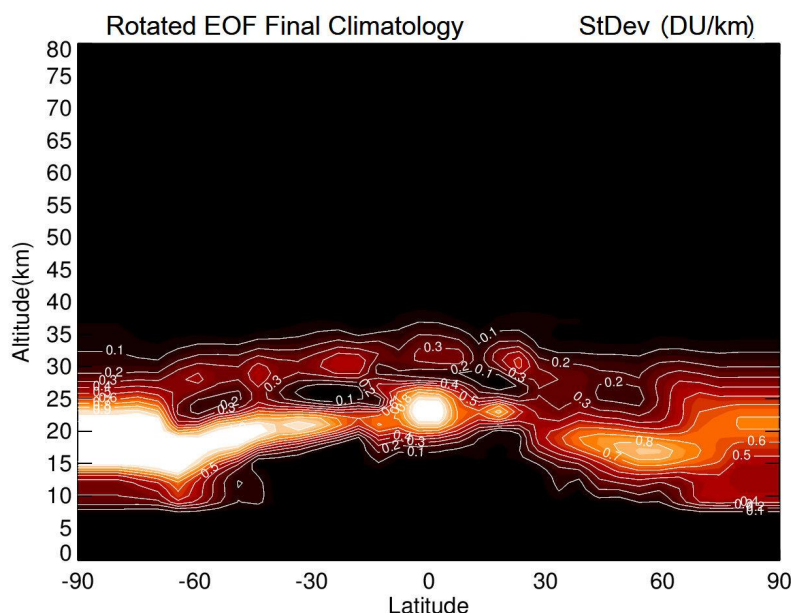
390

391 The REOF climatology was converted from the ozone partial pressures defined at 30 MLS levels
392 to volume mixing ratio (ppmv) and partial ozone column (DU km^{-1}) at the $1 \text{ km } Z^*$ levels
393 (defined in section 3.2) identical to the MLS/GMI climatology. The REOF climatological values
394 at levels below $\sim 9 \text{ km}$ and above $\sim 48 \text{ km}$ are very small in contributing to inter-annual
395 variability of ozone and are set to zero. Since the REOF climatology uses zonal wind and total
396 ozone time series that can have long-term trends, we applied a very low frequency (VLF) digital
397 low-pass filter to the final derived REOF climatology to remove long-term decadal variability.
398 This was done to ensure that the climatology captures only inter-annual variability in monthly
399 zonal mean ozone anomaly profiles without inducing decadal trends if used as a prior in ozone
400 retrieval. The frequency response of the applied VLF digital filter (Stanford and Ziemke, 1993)
401 is exactly 0.0 (1.0) at zero (Nyquist) frequency with amplitude 0.5 at frequency $0.00333 \text{ month}^{-1}$.

402

403 The magnitude of inter-annual variability in profile ozone captured by the REOF climatology is
404 shown in Fig. 6 as calculated standard deviations in DU km^{-1} for the 1970-2018 period. In the
405 tropical low latitudes from 10°S - 10°N the main source of inter-annual variability is the QBO.
406 However, larger inter-annual variability occurs in the SH extra-tropics due to the QBO and
407 additional dynamical sources. In an effort to understand the contribution of non-QBO processes
408 to the inter-annual variability we also generated a climatology based on using only equatorial
409 QBO zonal winds as a proxy (see Fig. S4 in the Supplementary Material). When compared to
410 the REOF climatology in Fig. 6, only a very small fraction of inter-annual variability is captured
411 in the extra-tropics for the QBO-only climatology.

412



413

414 **Figure 6.** Temporal standard deviation (in DU km^{-1}) for 1970-2018 for the final REOF ozone
415 climatology (i.e., Eq. (S10) in Supplementary Materials). The inter-annual variability in the
416 tropical low latitudes is almost entirely due to the QBO. Inter-annual variability in the extra-
417 tropics comes from the QBO coupled with other non-QBO related inter-annual variability.

418

419 The long record of the REOF inter-annual ozone profile climatology has been compared with de-
420 seasonalized ozone profile measurements from SAGE II and Aura MLS for 1984-2018 (Fig. 7).

421 The top panel in Fig. 7a shows comparisons of upper stratospheric column ozone anomalies
422 ($Z^* = 25\text{-}50$ km) between REOF (black curve) and SAGE (red asterisks) for years 1984-2005 in
423 the tropics ($10^\circ\text{S}\text{-}10^\circ\text{N}$). The bottom panel in Fig. 7b shows a similar comparison between
424 REOF and MLS for 2005-2018. Figure 7b is the same as in Fig. 7a, except for the lower
425 stratosphere ($Z^* = 17\text{-}25$ km).

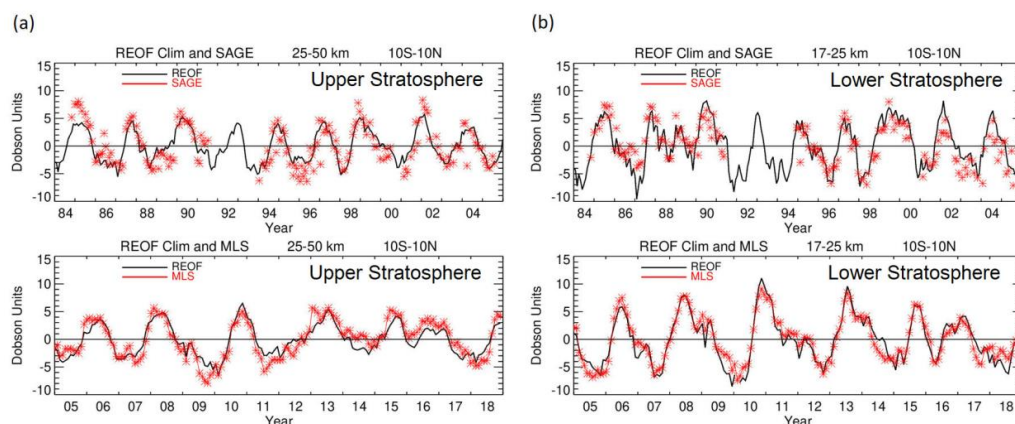
426

427 The SAGE II sampling ozone columns in Fig. 7 is sparse, averaging $\sim 2\text{-}3$ days of measurements
428 for a given month in the $10^\circ\text{S}\text{-}10^\circ\text{N}$ latitude band shown. This means that the monthly SAGE
429 measurements in Fig. 7 are more representative of daily profiles rather than monthly means.

430 Ozone profiles on a daily basis in the tropics are distorted by propagating tropical waves with



431 periods of days to weeks such as Kelvin waves, equatorial Rossby waves, and mixed Rossby-
432 gravity waves (e.g., Timmermans et al., 2005; Ziemke and Stanford, 1994). As a result, the
433 upper and lower stratospheric columns in Fig. 7 for SAGE II will have noisy month-to-month
434 variations of several DU because of these tropical waves. The Supplementary Material includes
435 further discussion and figures for the REOF climatology.
436



437
438 **Figure 7.** (a) Top panel is zonal-mean upper stratospheric column ozone (in Dobson Units) for
439 the REOF climatology (black curve) and deseasonalized SAGE II (red asterisks) spanning 1984-
440 2005 and averaged between 10°S-10°N. The SAGE data are deseasonalized monthly zonal
441 means. All column amounts are calculated by integrating ozone profiles for $Z^*=25-50$ km (~28
442 to 1 hPa). Bottom panel is the same as the top panel, but with MLS in place of SAGE and for the
443 time period 2005-2018. (b) Same as (a), but for the lower stratosphere with $Z^*=17-25$ km (~88
444 to 28 hPa).

445
446 **5. Summary.**

447
448 We have produced a new MLS/GMI seasonal ozone profile climatology by combining ozone
449 profiles from the M2GMI model simulation with MLS v4.2 measurements. M2GMI is used
450 primarily for tropospheric ozone and MLS for stratospheric ozone, with the two ozone profile
451 datasets blended together in the low stratosphere; the result is a merged zonal-mean, 12-month
452 global ozone profile climatology at 5° latitude resolution with Z^* altitude range 0-80 km (1 km



453 vertical sampling). Our main interest in generating the MLS/GMI climatology is to use it as a
454 priori information in satellite ozone retrieval algorithms. However, it is also useful as a baseline
455 for evaluating various modeled or measured ozone, and in studies involving atmospheric
456 radiative transfer calculations.

457

458 In previous studies we generated several ozone profile climatologies based on combining
459 ozonesondes with either SAGE or MLS satellite measurements (e.g., McPeters et al., 2007;
460 McPeters and Labow, 2012; Labow et al., 2015). We have compared the new MLS/GMI
461 climatology in detail with the ML climatology of McPeters and Labow (2012) that used
462 ozonesondes for tropospheric ozone profiles. The M2GMI model simulation provides an
463 improved ozone climatology for the troposphere compared to the ML climatology due to having
464 much better spatial and temporal coverage than the sondes.

465

466 We also developed a time-dependent climatology of monthly zonal-mean profile ozone
467 anomalies representing inter-annual variability. This inter-annual climatology was constructed
468 using a rotational EOF analysis of Aura MLS monthly zonal-mean profile ozone anomalies from
469 August 2004 – December 2016 within each 5° latitude band. The analysis shows that the first
470 two leading EOFs explain ~70-80% of inter-annual variability of profile ozone at all latitudes.
471 Furthermore, total ozone and tropical zonal wind time series correlate well with the two leading
472 EOF coefficient time series and were used as proxies to extend information outside the Aura
473 MLS time range. We used these relationships to reconstruct anomalies at 5° latitudinal resolution
474 for $Z^* = 0-80$ km and 1970-2018. This REOF time-dependent climatology was compared to a
475 similar climatology based on only tropical QBO winds. The advantage of the REOF climatology
476 is that allows for a much more thorough representation of inter-annual variability of stratospheric
477 ozone than just the QBO.

478

479 The REOF time-dependent climatology of ozone profile anomalies can be easily added to the
480 MLS/GMI seasonal climatology to simulate seasonal+inter-annual variability of stratospheric
481 ozone. We note that both the MLS/GMI 12-month climatology and REOF climatology were
482 generated using Aura time period MLS ozone measurements and neither of them account for
483 long-term trends in stratospheric ozone.



484

485

486 **Acknowledgments.** We thank the NASA Jet Propulsion Laboratory MLS team for the MLS
487 v4.2 ozone dataset and the SHADOZ, WOUDC and NDACC personnel for providing the
488 extensive ozonesonde measurements that we used for our study. We also thank the NASA MAP
489 program for supporting the MERRA-2 GMI simulation and the NASA Center for Climate
490 Simulation (NCCS) for providing high-performance computing resources. Special thanks go to
491 the NASA GMI group especially Sarah Strode regarding the MERRA-2 GMI simulation.
492 Funding for this research was provided in part by NASA NNH14ZDA001N-DSCOVER.

493

494

495 **Data availability.** Data description for MLS v4.2 ozone and links to the data can be obtained
496 from websites https://mls.jpl.nasa.gov/products/o3_product.php (last access 16 April 2021) and
497 <https://disc.gsfc.nasa.gov/> (last access 16 April 2021). MERRA-2 GMI model description and
498 access is available at <https://acd-ext.gsfc.nasa.gov/Projects/GEOSCCM/MERRA2GMI/> (last
499 access: 16 April 2021). The MOD total ozone measurements are available from the webpage
500 https://acd-ext.gsfc.nasa.gov/Data_services/merged/. Tropical QBO winds were provided by the
501 University of Berlin from <https://www.geo.fu-berlin.de/met/ag/strat/produkte/qbo/qbo.dat>. The
502 seasonal and inter-annual climatology products derived from our study are available for the
503 general public using direct links from the NASA webpage <https://avdc.gsfc.nasa.gov/>.

504

505

506 **References.**

507

508 Bass, A. M., and R. J. Paur, The ultraviolet cross-sections of ozone, I: The measurements, in
509 *Proc. Quad. Ozone Symp.*, edited by C. Zerefos, and A. Ghazi, pp. 606–616, Reidel, Dordrecht,
510 Halkidiki, Greece, 1984.

511

512 Bourgeois, I., J. Peischl, C. R. Thompson, K. C. Aikin, T. Campos, H. Clark, R. Commane, B.
513 Daube, G. W. Diskin, J. W. Elkins, R.-S. Gao, A. Gaudel, E. J. Hints, B. J. Johnson, R. Kivi, K.
514 McKain, F. L. Moore, D. D. Parrish, R. Querel, E. Ray, R. Sánchez, C. Sweeney, D. W.



- 515 Tarasick, A. M. Thompson, V. Thouret, J. C. Witte, S. C. Wofsy, and T. B. Ryerson, Global-scale
516 distribution of ozone in the remote troposphere from the ATom and HIPPO airborne field
517 missions *Atmos. Chem. Phys.*, 20, 10611–10635, <https://doi.org/10.5194/acp-20-10611-2020>,
518 2020.
- 519
- 520 Duncan, B. N., R. V. Martin, A. C. Staudt, R. Yevich, and J. A. Logan, Interannual and seasonal
521 variability of biomass burning emissions constrained by satellite observations, *J. Geophys. Res.*
522 *Atmos.*, 108(D2), doi:10.1029/2002jd002378, 2003.
- 523
- 524 Duncan, B.N., S.E. Strahan, Y. Yoshida, S.D. Steenrod, and N. Livesey, Model study of cross-
525 tropopause transport of biomass burning pollution, *Atmos. Chem. Phys.*, 7, 3713-3736,
526 doi:10.5194/acp-7-3713-2007, 2007.
- 527
- 528 Fishman, J., C. E. Watson, J. C. Larsen, and J. A. Logan, Distribution of tropospheric ozone
529 determined from satellite data, *J. Geophys. Res.*, 95(D4), 3599-3617, 1990.
- 530
- 531 Frith, S. M., N. A. Kramarova, R. S. Stolarski, R. D. McPeters, P. K. Bhartia, and G. J. Labow,
532 Recent changes in total column ozone based on the SBUV Version 8.6 Merged Ozone Data Set,
533 *J. Geophys. Res. Atmos.*, 119, 9735–9751, doi:10.1002/2014JD021889, 2014.
- 534
- 535 Frith, S. M., P. K. Bhartia, L. D. Oman, N. A. Kramarova, R. D. McPeters, and G. J. Labow,
536 Model-based climatology of diurnal variability in stratospheric ozone as a data analysis tool
537 *Atmos. Meas. Tech.*, 13, 2733–2749, <https://doi.org/10.5194/amt-13-2733-2020>, 2020.
- 538
- 539 Froidevaux, L., et al., Validation of Aura Microwave Limb Sounder stratospheric ozone
540 measurements, *J. Geophys. Res.*, 113, D15S20, doi:10.1029/2007JD008771, 2008.
- 541
- 542 Gelaro, R., W. McCarty, M.J. Suárez, R. Todling, A. Molod, L. Takacs, C.A. Randles, A.
543 Darmenov, M.G. Bosilovich, R. Reichle, K. Wargan, L. Coy, R. Cullather, C. Draper, S. Akella,
544 V. Buchard, A. Conaty, A.M. da Silva, W. Gu, G. Kim, R. Koster, R. Lucchesi, D. Merkova, J.E.
545 Nielsen, G. Partyka, S. Pawson, W. Putman, M. Rienecker, S.D. Schubert, M. Sienkiewicz, and



- 546 B. Zhao, The Modern-Era Retrospective Analysis for Research and Applications, Version 2
547 (MERRA-2), *J. Climate*, 30, 5419–5454, <https://doi.org/10.1175/JCLI-D-16-0758.1>, 2017.
548
- 549 Giglio, L., J. Randerson, and G. van der Werf, Analysis of daily, monthly, and annual burned
550 area using the fourth-generation global fire emissions database (GFED4), *J. Geophys. Res.*
551 *Bio.Sci.*, 118(1), 317-328, doi:10.1002/jgrg.20042, 2013.
552
- 553 Granier, C., B. Bessagnet, T. Bond, A. D'Angiola, H. D. van der Gon, et al., Evolution of
554 anthropogenic and biomass burning emissions of air pollutants at global and regional scales
555 during the 1980–2010 period. *Climatic Change*, 109, 163–190, doi:10.1007/s10584-011-0154-1,
556 2011.
557
- 558 Jaeglé, L., V. Shah, J. A. Thornton, F. D. Lopez-Hilfiker, B. H. Lee, E. E. McDuffie, et al.,
559 Nitrogen oxides emissions, chemistry, deposition, and export over the Northeast United States
560 during the WINTER aircraft campaign, *J. Geophys. Res. Atmos.*, 123, 12,368–12,393,
561 <https://doi.org/10.1029/2018JD029133/>, 2018.
562
- 563 Jiang, Y. B., et al., Validation of Aura Microwave Limb Sounder Ozone by ozonesonde and lidar
564 measurements, *J. Geophys. Res.*, 112, D24S34, doi:[10.1029/2007JD008776](https://doi.org/10.1029/2007JD008776), 2007.
565
- 566 Kutzbach, J. E., Empirical eigenvectors of sea-level pressure, surface temperature and
567 precipitation complexes over North America, *J. App. Meteorol.*, 6, 791-802,
568 [https://doi.org/10.1175/1520-0450\(1967\)006<0791:EEOSLP>2.0.CO;2](https://doi.org/10.1175/1520-0450(1967)006<0791:EEOSLP>2.0.CO;2), 1967.
569
- 570 Labow, G. J., J. R. Ziemke, R. D. McPeters, D. P. Haffner, and P. K. Bhartia, A total ozone-
571 dependent ozone profile climatology based on ozonesondes and Aura MLS data, *J. Geophys.*
572 *Res. Atmos.*, 120, 2537-2545, doi:10.1002/2014JD022634, 2015.
573
- 574 Lamarque, J.-F., T. C. Bond, V. Eyring, C. Granier, A. Heil, Z. Klimont, D. Lee, C. Liousse, A.
575 Mieville, B. Owen, M. G. Schultz, D. Shindell, S. J. Smith, E. Stehfest, J. Van Aardenne, O. R.



- 576 Cooper, M. Kainuma, N. Mahowald, J. R. McConnell, V. Naik, K. Riahi, and D. P. van Vuuren,
577 Historical (1850-2000) gridded anthropogenic and biomass burning emissions of reactive gases
578 and aerosols: methodology and application, *Atmos. Chem. Phys.*, 10(15), 7017-7039,
579 doi:10.5194/acp-10-7017-2010, 2010.
580
- 581 Livesey, N. J., Read, W. G., Froidevaux, L., Lambert, A., Manney, G. L., Pumphrey, H. C.,
582 Santee, M. L., Schwartz, M. J., Wang, S., Cofield, R. E., Cuddy, D. T., Fuller, R. A., Jarnot, R.
583 F., Jiang, J. H., Knosp, B. W., Stek, P. C., Wagner, P. A., and Wu, D. L.: *EOS MLS Version 3.3*
584 *Level 2 data quality and description document, Tech. rep., Jet Propulsion Laboratory*, available
585 at: <http://mls.jpl.nasa.gov/>, 2011.
586
- 587 McPeters, R. D., G. J. Labow, and J. A. Logan, Ozone climatological profiles for satellite
588 retrieval algorithms, *J. Geophys. Res.*, 112, D05308, doi:10.1029/2005JD006823, 2007.
589
- 590 McPeters, R. D., and G. J. Labow, Climatology 2012: An MLS and sonde derived ozone
591 climatology for satellite retrieval algorithms, *J. Geophys. Res.*, 117, doi:10.1029/2011JD017006,
592 2012.
593
- 594 McPeters, R. D., P. K. Bhartia, D. Haffner, G. J. Labow, and L. Flynn, The version 8.6 SBUV
595 ozone data record: An overview, *J. Geophys. Res.*, 118, 8032–8039, doi:10.1002/jgrd.50597,
596 2013.
597
- 598 Molod, A., L. Takacs, M. Suarez, and J. Bacmeister, Development of the GEOS-5 atmospheric
599 general circulation model: evolution from MERRA to MERRA2, *Geosci. Mod. Dev.*, 8,
600 doi:10.5194/gmd-8-1339-2015, 2015.
601
- 602 Oman, L. D., A. R. Douglass, J. R. Ziemke, J. M. Rodriguez, D. W. Waugh, and J. E. Nielsen,
603 The ozone response to ENSO in Aura satellite measurements and a chemistry-climate
604 simulation, *J. Geophys. Res.*, 118, 965-976, doi:10.1029/2012JD018546, 2013.
605



- 606 Orbe, C., L. D. Oman, S. E. Strahan, D. W. Waugh, S. Pawson, L. L. Takacs, and A. M. Molod,
607 Large-Scale Atmospheric Transport in GEOS Replay Simulations, *J. Adv. Mod. Earth Sys.*, 9,
608 2545-2560, 2017.
- 609
- 610 Park, J. H., M. K. Ko, C. H. Jackman, R. A. Plumb, J. A. Kaye, and K. H. Sage, Models and
611 Measurements Intercomparison II, *NASA Tech. Memo., NASA/TM-1999-209554*, 502 pp., 1999.
- 612
- 613 Parrish, A., Boyd, I. S., Nedoluha, G. E., Bhartia, P. K., Frith, S. M., Kramarova, N. A., Connor,
614 B. J., Bodeker, G. E., Froidevaux, L., Shiotani, M., and Sakazaki, T.: Diurnal variations of strato-
615 spheric ozone measured by ground-based microwave remote sensing at the Mauna Loa NDACC
616 site: measurement validation and GEOSCCM model comparison, *Atmos. Chem. Phys.*, 14, 7255–
617 7272, <https://doi.org/10.5194/acp-14-7255-2014>, 2014.
- 618
- 619 Richman, M. B., Rotation of principal components, *J. Clim.*, 6, 293-335,
620 <https://doi.org/10.1002/joc.3370060305>, 1986.
- 621
- 622 Rodgers, C. D., Inverse methods for atmospheric sounding: theory and practice, *World Scientific*
623 *Publishing Co., pp. 238*, London, United Kingdom, 2000.
- 624
- 625 Shepherd, T. G., D. A. Plummer, J. F. Scinocca, M. I. Hegglin, V. E. Fioletov, M. C. Reader, E.
626 Remsberg, T. von Clarmann, and H. J. Wang, Reconciliation of halogen-induced ozone loss with
627 the total-column ozone record, *Nature Geosci.*, 7, doi:10.1038/NGEO2155, 2014.
- 628
- 629 Stanford, J. L., J. R. Ziemke, and S. Y. Gao, Stratospheric circulation features deduced from
630 SAMS constituent data, *J. Atmos. Sci.*, 50, 226-246, 1993.
- 631
- 632 Stauffer, R. M., A. M. Thompson, L.D. Oman, and S.E. Strahan, The effects of a 1998 observing
633 system change on MERRA-2-based ozone profile simulations. *J. Geophys. Res. Atmos.*, 124,
634 7429-7441, <https://doi.org/10.1029/2019JD030257>, 2019.
- 635



- 636 Strode, S. A., J. M. Rodriguez, J. A. Logan, O. R. Cooper, J. C. Witte, L. N. Lamsal, M. Damon,
637 B. Van Aartsen, S. D. Steenrod, and S. E. Strahan, Trends and variability in surface ozone over
638 the United States, *J. Geophys. Res. Atmos.*, *120*(17), 9020-9042, doi:10.1002/2014JD022784,
639 2015.
640
- 641 Strode, S. A., J. S. Wang, M. Manyin, B. N. Duncan, R. Hossain, C. A. Keller, S. E. Michel, and
642 J. W. C. White, Strong sensitivity of the isotopic composition of methane to the plausible range
643 of tropospheric chlorine, *Atmos. Chem. Phys.*, *20*, 8405–8419, [https://doi.org/10.5194/acp-20-](https://doi.org/10.5194/acp-20-8405-2020)
644 [8405-2020](https://doi.org/10.5194/acp-20-8405-2020), 2020.
645
- 646 Thompson, A. M., Witte, J. C., Sterling, C., Jordan, A., Johnson, B. J., Oltmans, S. J., Fujiwara,
647 M., Vömel, H., Allaart, M., Pitters, A., Coetzee, G. J. R., Posny, F., Corrales, E., Andres Diaz, J.,
648 Félix, C., Komala, N., Lai, N., Maata, M., Mani, F., Zainal, Z., Ogino, S.-Y., Paredes, F., Luiz
649 Bezerra Penha, T., Raimundo da Silva, F., Sallons-Mitro, S., Selkirk, H. B., Schmidlin, F. J.,
650 Stuebi, R., and Thiongo, K.: First reprocessing of Southern Hemisphere Additional Ozonesondes
651 (SHADOZ) Ozone Profiles (1998–2016). 2. Comparisons with satellites and ground-based
652 instruments, *J. Geophys. Res.*, *122*, 13000–13025, <https://doi.org/10.1002/2017JD027406>, 2017.
653
- 654 Timmermans, R. M. A., R. F. van Oss, and H. M. Kelder, Equatorial Kelvin wave signatures in
655 ozone profile measurements from Global Ozone Monitoring Experiment (GOME), *J. Geophys.*
656 *Res.*, *110*, D21103, doi:10.1029/2005JD005929, 2005.
657
- 658 Wallace, J. M., R. L. Panetta, and J. Estberg, Representation of the equatorial stratospheric
659 Quasi-Biennial Oscillation in EOF phase space, *J. Atmos. Sci.*, *50*, 12, 1751-1762,
660 doi:10.1175/1520-0469(1993)050<1751:ROTESQ>2.0.CO;2, 1993.
661
- 662 Wargan, K., C. Orbe, S. Pawson, J. R. Ziemke, L. D. Oman, M. A. Olsen, et al., Recent decline
663 in extratropical lower stratospheric ozone attributed to circulation changes. *Geophys. Res. Lett.*,
664 *45*, 5166–5176. [https:// doi.org/10.1029/2018GL077406](https://doi.org/10.1029/2018GL077406), 2018.
665



- 666 Witte, J. C., Thompson, A. M., Smit, H. G. J., Fujiwara, M., Posny, F., Coetzee, G. J. R.,
667 Northam, E. T., Johnson, B. J., Sterling, C. W., Mohammed, M., Ogino, S.-Y., Jordan, A.,
668 daSilva, F. R., and Zainal, Z.: First reprocessing of Southern Hemisphere Additional
669 OZonesondes (SHADOZ) profile records (1998–2015) 1: Methodology and evaluation, *J.*
670 *Geophys. Res.*, *122*, 6611–6636, <https://doi.org/10.1002/2016JD026403>, 2017.
- 671
- 672 Ziemke, J. R., and J. L. Stanford, Quasi-biennial oscillation and tropical waves in total ozone, *J.*
673 *Geophys. Res.*, *99*, 23,041-23,056, 1994.
- 674 Ziemke, J. R., S. Chandra, A. Thompson, and D. McNamara, Zonal asymmetries in Southern
675 Hemisphere column ozone: Implications of biomass burning, *J. Geophys. Res.*, *101*, 14,421-
676 14,427, doi:10.1029/96JD01057, 1996.
- 677 Ziemke, J. R., S. Chandra, G. J. Labow, P. K. Bhartia, L. Froidevaux, and J. C. Witte, A global
678 climatology of tropospheric and stratospheric ozone derived from Aura OMI and MLS
679 measurements, *Atmos. Chem. Phys.*, *11*, 9237-9251, doi:10.5194/acp-11-9237-2011, 2011.
- 680
- 681 Ziemke, J. R., M. A. Olsen, J. C. Witte, A. R. Douglass, S. E. Strahan, K. Wargan, X. Liu, M. R.
682 Schoeberl, K. Yang, T. B. Kaplan, S. Pawson, B. N. Duncan, P. A. Newman, P. K. Bhartia, M. K.
683 Heney, Assessment and applications of NASA ozone data products derived from Aura
684 OMI/MLS satellite measurements in context of the GMI Chemical Transport Model, *J. Geophys.*
685 *Res. Atmos.*, *119*, 5671-5699, doi:10.1002/2013JD020914, 2014.
- 686